

Gold supported on Cu–Mg–Al-mixed oxides: Strong enhancement of activity in aerobic alcohol oxidation by concerted effect of copper and magnesium

Peter Haider, Alfons Baiker*

Institute for Chemical and Bioengineering, Department of Chemistry and Applied Biosciences, ETH Zürich, Hönggerberg, HCI, CH-8093 Zürich, Switzerland

Received 7 February 2007; revised 8 March 2007; accepted 8 March 2007

Available online 20 April 2007

Abstract

Gold nanoparticles were deposited on mixed oxides containing Cu, Mg, and Al in different ratios. The mixed-oxide supports were prepared by flame spray pyrolysis (FSP), resulting in agglomerated primary nanoparticles in the 10–15 nm range, onto which 6- to 9-nm gold particles were deposited by means of deposition–precipitation. The mixed-oxide-supported Au catalysts with noble metal loading of 0.6 ± 0.17 wt% were investigated concerning their structural properties and tested in the aerobic liquid-phase oxidation of 1-phenylethanol to phenyl–methyl ketone affording TOFs up to 1300 h^{-1} . The catalytic tests showed that the activity of these catalysts depends strongly on the composition of the support, with Cu and Mg being crucial components. Strongly enhanced catalytic activity was observed for gold supported on a ternary mixed oxide containing Cu, Mg, and Al at the molar ratio of 5:1:2. Extension of the catalytic tests to various structurally different alcohols indicated that the ternary mixed-oxide-supported gold catalyst has excellent catalytic properties in the aerobic oxidation of a broad range of structurally different alcohols, affording selectivities $\geq 98\%$. XANES revealed both reduced and oxidized Au species on the ternary mixed-oxide supports before and after the reaction. CO_2 adsorption from the liquid phase combined with in situ ATR-IR and modulation excitation spectroscopy was applied to investigate differences in the basic surface properties of the mixed oxides. Monodentate and bidentate carbonates were identified, the former being dominant on ternary Cu-containing supports.

© 2007 Elsevier Inc. All rights reserved.

Keywords: Gold; Ternary Cu–Mg–Al-mixed oxides; Aerobic oxidation; Alcohols; Flame spray pyrolysis; CO_2 adsorption; ATR-IR; Basic support

1. Introduction

Gold-based catalysts can be used in various important reactions (see, e.g., [1] and references therein), including (preferential) CO oxidation of CO [2–5], synthesis of H_2O_2 [6], partial oxidation of alkenes [7], epoxidation of propylene [8,9], and oxidation of alcohols with O_2 . Supported Au catalysts and “naked” gold particles were reported to achieve high conversion and selectivity in the oxidation of various diols [10–12] and glucose [13–15]. Recently, the potential of using Au as an oxidation catalyst for the continuous oxidation of glucose was studied; in a long-term experiment, a low-loaded Au/ Al_2O_3 cat-

alyst was tested for 70 days and demonstrated no loss of activity [16,17].

It has been shown that the rate-limiting step for the oxidation of alcohols on various noble metals is a dehydrogenation step. Detailed investigations into this aspect have been previously performed by our group [18,19]. A base is often required to facilitate the dehydrogenation step, which can be alternatively achieved using basic mixed-oxide supports [20,21]. Supports with a Mg/Al molar ratio of 3:1 have been shown to be optimal for dehydrogenation reactions [22] and thus are used as supports for Au nanoparticles.

More recently, Au/ CeO_2 [23] and Au/ TiO_2 [24,25] have been proposed as catalysts for the oxidation of various aromatic and aliphatic alcohols achieving high turnover frequencies (TOFs). Improved selectivity was achieved by applying supported alloyed Au/Pd particles. The promotional effect of

* Corresponding author.

E-mail address: baiker@chem.ethz.ch (A. Baiker).

alloying has also been described for unsupported alloyed Au particles in the oxidation of glucose [26]. The oxidation of an aqueous ethanol solution has been successfully performed on Au deposited on an MgAl_2O_4 spinel [27].

To the best of our knowledge, mixed oxides based on Cu, Mg, and Al have not yet been investigated as supports of Au nanoparticles in catalytic oxidation. Intrigued by the activity of hydrotalcites and hydrotalcite-like materials for dehydrogenation reactions at elevated temperatures [21,22] and by the beneficial effect of Cu on catalytic activity [28], we prepared a series of binary CuAl- and MgAl- and ternary CuMgAl-mixed-oxide supports by flame spray pyrolysis (FSP). The present work focused on exploring the potential of these materials in the gold-catalyzed aerobic oxidation of various structurally different alcohols.

2. Experimental

2.1. Preparation of supports and catalysts

The ternary $\text{Cu}_a\text{Mg}_b\text{Al}_c\text{O}_x$ and binary $\text{Mg}_3\text{Al}_1\text{O}_x$ and $\text{Cu}_3\text{Al}_1\text{O}_x$ mixed-oxide supports¹ were prepared by FSP. In the notation $\text{Cu}_a\text{Mg}_b\text{Al}_c\text{O}_x$, the subscripts *a*, *b*, and *c* indicate the molar ratio of Cu:Mg:Al = *a*:*b*:*c*. A detailed description of the experimental setup and the procedure applied has been provided previously [29,30]. In a typical experiment, the solution (a 2:1 v/v mixture of acetic acid and methanol) containing the precursors $\text{Al}(\text{C}_5\text{H}_7\text{O}_2)_3$, $\text{Cu}(\text{NO}_3)_2 \cdot 3\text{H}_2\text{O}$, and $\text{Mg}(\text{NO}_3)_2 \cdot 6\text{H}_2\text{O}$ in the desired concentrations was fed with a syringe pump (6 mL/min) into the spray nozzle and dispersed with oxygen. The total concentration of metal ions in the feed was 0.5 mol/L. Binary 20 wt% CuO/CeO₂ used to explore the promoting action of copper was prepared accordingly but from corresponding nitrates as precursor salts. The pressure drop was set to a constant value of 1 bar at the nozzle tip, and the oxygen flow rate (5 L/min) was controlled with a mass flow controller. The aerosol was ignited by a small flame ring issuing from an annular gap (0.15 mm spacing, 6 mm radius). The gas flow rate of this premixed oxygen/methane supporting flame was 1.75 L/min (0.75 L/min CH₄ and 1 L/min O₂). Powder collection was performed with a glass fiber filter using a vacuum pump. Reference supports applied were CeO₂, purchased from MCT Microcoating Technologies, and TiO₂ (P25), purchased from Degussa. Both supports were used as received from the suppliers.

Gold was deposited on the different binary and ternary mixed-oxide supports by deposition–precipitation following a procedure reported by Haruta [2]. Typically, about 1 g of the well-ground support was suspended in 80 mL of deionized water and brought to pH 9–11 with freshly prepared 0.2 N NaOH. The corresponding volume of HAuCl₄ solution containing the desired amount of Au was taken out of a stock solution, poured into 20 mL of deionized water, and brought

to pH 9–11 with 0.2 N NaOH. The Au precursor was stirred for 15 min, which resulted in almost total disappearance of the yellow color, and then mixed with the suspension of the support. After stirring, the catalyst was filtered off and washed extensively with deionized water until no traces of Cl[−] could be detected (AgNO₃ test). The catalyst was dried for 18 h at 80 °C and used without further pretreatment. The nominal gold content of the mixed-oxide-supported catalysts was 1 wt%, but because of some loss during preparation, the final Au content was 0.6 ± 0.17 wt%, depending on the support. Au/TiO₂ was prepared by impregnation of TiO₂ with HAuCl₄ and calcination at 400 °C for 4 h. Other reference catalysts used were 5 wt% Pd/Al₂O₃, supplied by Johnson Matthey, and a corresponding 0.75 wt% Bi-promoted Pd catalyst prepared according to recipe reported previously [31,32].

2.2. Catalyst properties

Nitrogen adsorption experiments were carried out at 77.3 K on a Micrometrics ASAP 2000 instrument using the BET and BJH methods. Before measurements, samples were outgassed at 423 K under vacuum conditions. Elemental analysis was performed using laser ablation ion-coupled plasma mass spectrometry. Ablation was performed using an excimer laser (Lambda Physik Compex 110 I; ArF, 193 nm; pulse energy, 150 mJ; frequency, 10 Hz) with a spot diameter of 40 μm. The resulting sample aerosol was carried by a helium stream into a mass spectrometer (Perkin-Elmer Elan 6100); calibration was performed using NIST 610 standards. (Further details about the instrumentation are available elsewhere [33,34].) As a complementary method, atomic adsorption spectrometry, using a Varian 220FS device, was used to determine the Au content. Au was leached from the catalysts using aqua regia (typically 10 mg of catalyst in 5–10 mL of aqua regia) and injected into a C₂H₂/O₂ flame. Calibration was performed by diluting an Au standard to the desired concentrations. The gold content of the mixed-oxide-supported catalysts was 0.6 ± 0.17 wt%. All TOF calculations were based on 0.6 wt% Au, thus representing conservative estimates.

For transmission electron microscopy (TEM) investigations, a suspension of the flame-made material in ethanol was deposited onto a carbon-coated copper grid. The microscope (Tecnai F30 FEI, with a field emission cathode, operating at 300 keV, with a point resolution of <2 Å) was also equipped with a high-angle annular dark field (HAADF) detector for scanning transmission electron microscopy (STEM) and an energy-dispersive X-ray (EDX) detector. This instrumentation is capable of detecting even very small metal particles (<1 nm) by Z contrast and of analyzing selected points by EDX spectroscopy.

2.3. Catalytic tests

Catalytic tests were performed at 90 °C using 50 mg of each catalyst and 2 mmol 1-phenylethanol in 2 mL of mesitylene as a test substrate. To achieve a similar substrate-to-noble metal ratio for the Pd-containing catalysts, the conditions were

¹ Note that the support contained significant amounts of carbonates due to the high partial pressure of CO₂ in the quenching zone of the flame, favoring the formation of carbonates.

changed slightly to 10 mg of catalyst and 7 mmol of 1-phenylethanol. Oxygen (50 mL/min) was bubbled through the vigorously stirred liquid at atmospheric pressure. The flow was regulated by a mass flow controller. Samples were taken during and at the end of every experiment, filtered, and diluted with isopropanol for subsequent gas chromatography analysis (Thermo Quest Trace 2000 using a HP-FFAP capillary column and a flame ionization detector). Tetradecane or ethylene glycol diacetate was added as an internal standard in all reactions. Average TOFs (site-time yields) were calculated based on all Au atoms contained in the catalysts at full conversion [35],

$$\text{TOF} = \frac{n_{\text{ROH}}}{n_{\text{Au}} \times t}$$

The selectivity was calculated according to

$$S(\%) = \frac{n_{\text{product}}}{n_{\text{converted}}} \times 100\%$$

that is, the percentage of the desired product among all converted molecules. The duration of each experiment is indicated in Table 1. Note that for the Bi (0.75 wt%)-promoted 5 wt% Pd/Al₂O₃ catalyst, only the Pd loading was taken into consideration when calculating the TOF. Linear fits in the Hammett plot were obtained from the algorithm implemented in Origin software, version 7.03 (OriginLab Corp.).

Alcohols used for test reactions were 1-phenylethanol (99%, Aldrich), benzyl alcohol (99%, Fluka), 4-nitrobenzyl alcohol (99%, Acros), 4-methylbenzyl alcohol (99%, ABCR), 4-chlorobenzyl alcohol (99%, Acros), 4-*tert*-butyl benzyl alcohol (99%, Merck), cyclohexanol (99%, Fluka), *o*-methyl-cyclohexanol (99%, Acros), 4-methyl-cyclohexanol (99%, ABCR), cinnamyl alcohol (97%, Fluka), 4-methoxybenzyl alcohol (98%, Acros), 1-(4-chlorophenyl)ethanol (98%, Aldrich), 1-phenyl-1-propanol (97%, Aldrich), 2-phenyl-1-propanol (97%, Acros), 3-phenyl-1-propanol (98%, Fluka), 9-fluorenone (98%, Lancaster), 1-octanol and 3-octanol (99%+, Acros), geraniol (98%, ABCR), and citronellol (96%, ABCR). Mesitylene (99%, Acros/Fluka) was used as a solvent, and tetradecane (99%, Fluka) and ethylene glycol diacetate (99%, Aldrich) served as internal standards.

2.4. CO₂ adsorption combined with modulation excitation spectroscopy ATR-IR spectroscopy

CO₂ was used as a probe molecule to characterize the basic properties of the mixed-oxide-supported Au catalysts. Species were identified using ATR-IR spectroscopy combined with modulation excitation spectroscopy (MES) [36–38], with the system periodically modulated/disturbed by changing a variable of interest within a modulation frequency in the range of mHz. A system perturbed with a certain frequency will respond at the modulation frequency (or higher harmonics thereof) and possibly exhibit a phase lag in the response [39]. The phase-resolved spectra were then calculated from the time-resolved spectra using the following equation:

$$A_k^{\text{PSD}}(\tilde{\nu}) = \frac{2}{T} \int_0^T A(\tilde{\nu}, t) \sin(k\omega t + \Phi_k^{\text{PSD}}) dt,$$

where $A(\tilde{\nu}, t)$ is the time-resolved ATR spectrum, $A_k^{\text{PSD}}(\tilde{\nu})$ is the phase-resolved spectrum, and Φ_k^{PSD} is the phase angle. For $\Phi_k^{\text{PSD}} = 0^\circ$, the spectrum is referred to as the in-phase spectrum; for $\Phi_k^{\text{PSD}} = 90^\circ$, it is called the out-of-phase spectrum. T is the modulation period, and $k\omega$ refers to the demodulation frequency, with $k = 1$ being the fundamental and $k > 1$ being the higher harmonics.

The measurements were performed using a Bruker Equinox 55 IR spectrometer equipped with a MCT detector and a homemade cell as described in detail elsewhere [40]. The catalyst (2–4 mg) was suspended in water and deposited on the ZnSe crystal. In a typical experiment, toluene was saturated with the desired gases and pumped through the cell using a peristaltic pump (ISMATEC ISM827) at a rate of 0.56 mL/min. First, N₂-saturated toluene was pumped through the measurement cell at 80 °C for 90 min before adsorbing CO₂ by flowing CO₂-saturated toluene for 60 min. After this period, the modulation experiments were started. The modulation periods ranged from 408.3 to 1633.2 s, depending on the catalytic system. One stimulation period was composed of 60 spectra obtained by co-adding 50–200 scans. Generally, 6–8 stimulation periods, depending on the modulation period, were recorded, with the first three periods not used for data acquisition [39]. All spectra presented here were demodulated at the fundamental frequency, that is, $k = 1$.

2.5. XANES experiments

Ex situ XANES spectra were recorded at ANKA (Forschungszentrum Karlsruhe; 2.5 GeV; 130 mA injection current; ANKA-XAS beamline) using a Si(111) double-crystal monochromator detuned to about 60% of the maximum intensity. An ionization chamber was used to determine the incoming X-ray intensity. Due to the low loading of the noble metals, the experiments were performed in fluorescence mode. A five-element Ge solid-state detector (Canberra) was applied to measure the fluorescence X-rays of the Au L alpha fluorescence line as function of the excitation energy. For this purpose, the sample was pressed as a pellet and positioned in a 45° angle in the beam. Cr filters were used to minimize the fluorescence X-rays of the matrix [41].

3. Results and discussion

3.1. Syntheses and characterization of the materials

The binary (CuAl, MgAl) and ternary (CuMgAl) mixed-oxide supports were prepared by means of FSP. There are numerous parameters affecting the homogeneity, size, morphology, and crystallinity of the materials obtained by this synthesis method. However, certain key parameters like the enthalpy density in the flame (kJ/g_{gas}) have been identified. Moreover, the so-called equivalence ratio (β , Eq. (1)) with \dot{n}_{oxidant} and \dot{n}_{fuel} representing the molar fluxes of the oxidant O₂ and the fuel, respectively, was found to affect the product formed in the flame [30,42,43]. For the preparation of the mixed-oxide supports, a high enthalpy density of 11.8 kJ/g_{gas} together with an

Table 1
Catalytic data obtained from the oxidation of various alcohols

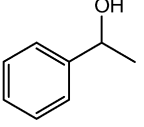
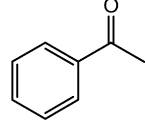
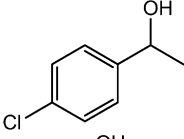
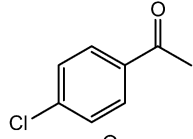
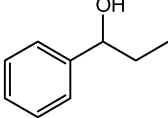
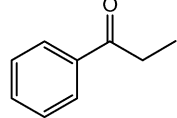
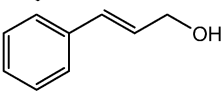
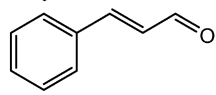
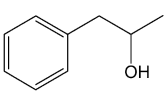
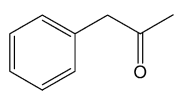
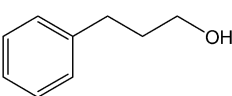
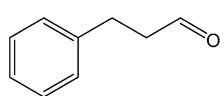
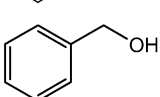
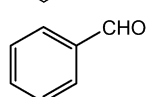
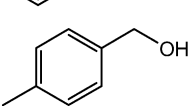
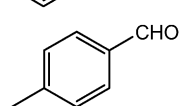
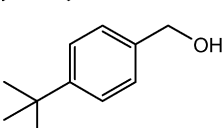
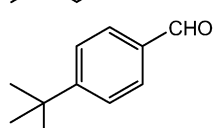
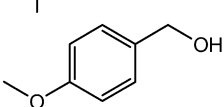
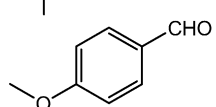
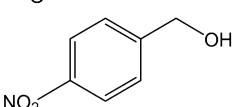
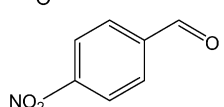
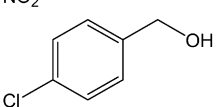
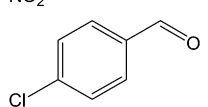
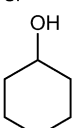
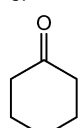
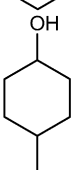
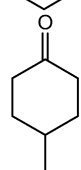
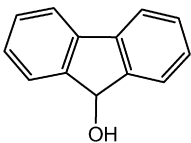
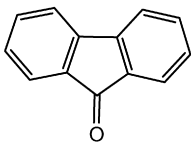
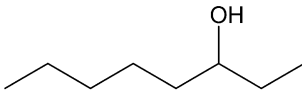
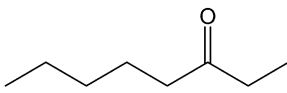
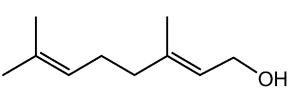
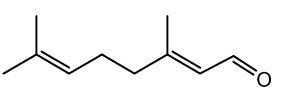
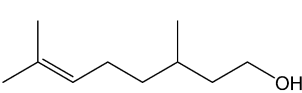
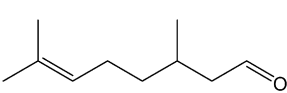
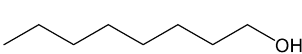
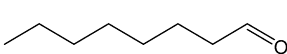
Reactant	Product	Time (h)	Yield (%)	Selectivity (%)	TOF (h^{-1})	Substrate/Au molar ratio
		1	99	>99	1294	1306
		2	99	>99	510	1030
		2	98	>99	527	1078
		2	>99	99	243	484
		4	36	99	20	220
		4	38	>99	20	212
		3	98	>99	130	397
		4	98	>99	129	528
		1	99	>99	333	336
		1, 5	99	>99	387	587
		1	>99	>99	98	98
		2	>99	99	47	93
		1	74	>99	166	225
		1	93	>99	147	158

Table 1 (continued)

Reactant	Product	Time (h)	Yield (%)	Selectivity (%)	TOF (h ⁻¹)	Substrate/Au molar ratio
		1	>99	99	421	421
		3	99	>99	85	257
		2	93	99	53	113
		2	36	98	28	152
		3	34	98	11	95

Note. Average TOFs (site-time yields) are calculated based on the total amount of Au present in the sample, thus representing conservative estimates. Conditions: 90 °C, 50 mL/min O₂, 50 mg catalyst, 2 mL mesitylene. Substrate/Au molar ratios are indicated in the table.

equivalence ratio of $\beta \approx 0.86$ was chosen to meet the proposed conditions

$$\beta = \frac{\left(\frac{\dot{n}_{\text{oxidant}}}{\dot{n}_{\text{fuel}}}\right)_{\text{stoichiometric}}}{\left(\frac{\dot{n}_{\text{oxidant}}}{\dot{n}_{\text{fuel}}}\right)_{\text{real}}} \quad (1)$$

Fig. 1 shows adsorption–desorption isotherms of some flame-derived binary and ternary mixed oxides and their corresponding differential pore size distributions. This type of isotherm was typical for all flame-derived mixed oxides investigated. A slight hysteresis was observed at higher relative pressures due to the interparticle void space between the agglomerated particles. The BET surface area was ca. 81 m²/g for the ternary Cu₅Mg₁Al₂O_x support and the binary Cu₃Al₁O_x material, while the Mg₃Al₁O_x support exhibited a larger surface area of 109 m²/g. The pore size distributions indicate that the flame-made particles had only slight porosity due to some small pores in the micropore and lower-mesopore range (the micropore area determined from the *t*-plot never exceeded 12 m²/g). Thus, we conclude that despite wide variety of chemical compositions, the mixed oxides had similar textural properties.

Representative TEM images of the structure of the Au-free ternary mixed-oxide support (Cu₅Mg₁Al₂O_x) are shown in Fig. 2 (top). The support exhibited a narrow particle size distribution with primary particle sizes in the 10–15 nm range. No larger particles were observed in all TEM images recorded. The support was mostly amorphous, but some crystalline regions were also discernible.

The size of the gold particles deposited on the ternary mixed-oxide support was in the range of 6–9 nm as measured by HAADF-STEM (Fig. 2, bottom). Most of the gold particles were spherical-shaped, but some irregular-shaped particles were also identified. Although different supports are known to lead to different particle sizes at the same gold loading, the particle dimensions reported here are in good agreement

with the literature data [10,11,14,44,45]. Larger Au particles (mean diameter ca. 25 nm) [46] and even larger AuPd particles (>60 nm) [24] also have been reported. Interestingly, we found that the deposition of smaller Au particles via a colloidal route previously used in our group [4,5] yielded less active catalysts than those obtained by deposition–precipitation. However, a conclusive statement regarding the influence of particle size on activity awaits further investigations with preparation procedures leading to very narrow and tunable particle size distributions. Studies in this regard are currently underway in our laboratory.

Elemental mapping was performed using HAADF-STEM, which allows the detection of heavy elements (Au) in a matrix of the lighter elements like Cu, Mg, or Al. To unambiguously assign the gray scales to the corresponding elements, three small areas were analyzed with the EDX technique. Fig. 3 shows a few very bright spots attributed to Au particles, along with large areas exhibiting different gray scales ascribed to well-dispersed nonaggregated Cu, Mg, and Al.

To gain some information about the oxidation state of Au in the ternary mixed-oxide-supported catalysts, XANES spectra were recorded. Due to interference of Cu (Cu K-edge, 8979 eV) and Au (Au L₃-edge, 11919 eV), a sample with lower Cu content (Au/Cu₃Mg₃Al₂O_x) was analyzed by fluorescence XANES (Fig. 4). Both the fresh and the used catalyst were analyzed without further pretreatment, and both exhibited large, intense white lines. In the Au/Cu₃Mg₃Al₂O_x catalyst, a significant amount of Au was found in the oxidized state; even after reaction, a considerable amount of Au was still in a Au³⁺ oxidation state. The observed white line was too intense to be caused by ligand or size effects that have been described for Au nanoparticles in the 1.6- to 4-nm range [47] and for smaller Au clusters down to 11 atoms [48]. Comparing our spectra with those reported previously [47–49] leads us to confidently conclude that the high intensity of the white line is due to the oxidation state, not to other effects. Moreover, the correspond-

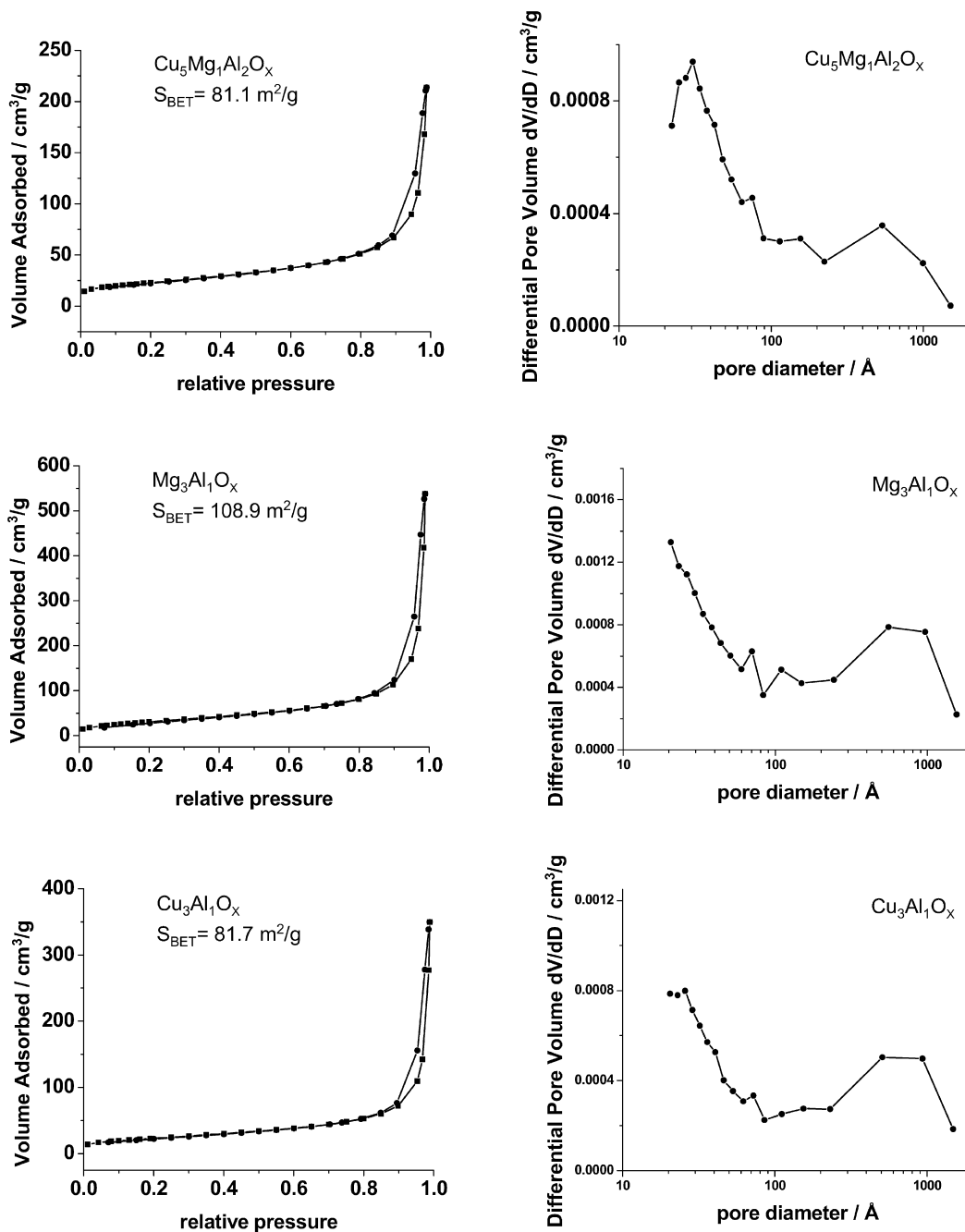


Fig. 1. Nitrogen adsorption–desorption isotherm of flame-synthesized ternary ($\text{Cu}_5\text{Mg}_1\text{Al}_2\text{O}_x$) and binary ($\text{Mg}_3\text{Al}_1\text{O}_x$ and $\text{Cu}_3\text{Al}_1\text{O}_x$) mixed-oxide supports (left). The corresponding differential pore size distributions calculated from the desorption isotherms are shown on the right.

ing post-edge pattern has not been transformed into the pattern observed for metallic gold, as was the case for the Au/CeO_2 system.

Note that unlike other metals, the XANES spectra at the Au L_3 -edge exhibit an apparent shift in the position of the main edge of Au^{3+} (d^8) toward lower energies with respect to Au^0 [50,51], due to an overlap of a very intense pre-edge feature and the actual edge itself [52]. This effect does not appear when the Au L_1 -edge is monitored [53]. Further investigations dealing with in situ experiments of these two systems are currently underway to gain deeper insight into the active Au species in alcohol oxidation.

3.2. Catalytic behavior

The effect of the composition of the support on the catalytic performance of the mixed-oxide-supported Au catalysts in the oxidation of 1-phenylethanol is shown in Fig. 5. Note that all supports had the same $(\text{Cu} + \text{Mg})/\text{Al}$ molar ratio of 3:1 but different Cu/Mg molar ratios. A maximum phenyl–methyl ketone yield was observed for samples with a molar ratio $\text{Cu}/\text{Mg} = 5:1$, indicating that both components contribute to enhanced activity. With all samples, no significant byproduct formation was observed. Note that the reaction also proceeded with the binary $\text{Mg}_3\text{Al}_1\text{O}_x$ and $\text{Cu}_3\text{Al}_1\text{O}_x$ supports, but at much lower reaction

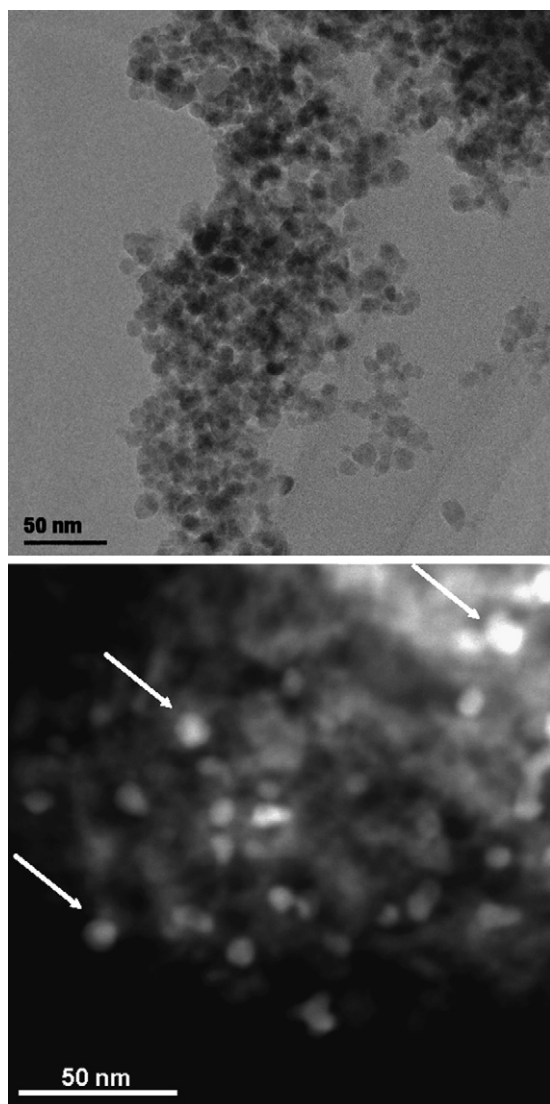


Fig. 2. Top: structural properties of ternary mixed oxide $\text{Cu}_5\text{Mg}_1\text{Al}_2\text{O}_x$ as observed by TEM; bottom: HAADF-STEM investigation of corresponding gold-loaded catalyst $\text{Au}/\text{Cu}_5\text{Mg}_1\text{Al}_2\text{O}_x$. Au particles in the size range of 6–9 nm are discernible. Au particles are bright in the HAADF-STEM image (Z contrast).

rates, indicating a synergistic effect of these promoting components. The pure supports contained ionic Cu^{2+} as determined by means of XANES (spectra not shown). All Au-free Mg-containing supports were virtually inactive, whereas $\text{Cu}_3\text{Al}_1\text{O}_x$ showed slight activity (ca. 2% yield).

The activity of the $\text{Au}/\text{Cu}_5\text{Mg}_1\text{Al}_2\text{O}_x$ catalyst was compared with that of other Au- and Pd-based reference catalysts. The binary mixed-oxide-supported $\text{Au}/\text{Mg}_3\text{Al}_1\text{O}_x$ exhibited activity similar to that of $\text{Pd}/\text{Al}_2\text{O}_3$ and Au/CeO_2 , which were previously reported to be active catalysts for the oxidation of alcohols. The Au/CeO_2 catalyst based on a commercially available CeO_2 reached an average $\text{TOF}_{(t=0.5\text{ h})} = 526\text{ h}^{-1}$ comparable to that observed previously at similar conditions [23]. However, replacement of some of the Mg by Cu (ternary mixed oxide) led to a dramatic increase in the catalytic activity, reaching the performance of Bi-promoted $\text{Pd}/\text{Al}_2\text{O}_3$ (Fig. 6) [54,55].

To gain some information on the scope of application of the most active $\text{Au}/\text{Cu}_a\text{Mg}_b\text{Al}_c\text{O}_x$ catalyst ($\text{Au}/\text{Cu}_5\text{Mg}_1\text{Al}_2\text{O}_x$), the oxidation of various structurally different alcohols was tested. The catalytic results summarized in Table 1 indicate a high versatility of the ternary mixed-oxide-supported gold catalyst. The oxidation of activated alcohols that allow stabilization of the adsorbed alkoxy-species showed high average TOFs, ranging up to 1296 h^{-1} for 1-phenylethanol. The other aromatic alcohols had TOFs ranging from 47 to 387 h^{-1} , depending on the substituents. Electron-withdrawing groups like chloro- and nitro-groups led to a decrease in activity, as did 1-(4-chlorophenyl)-ethanol, 4-chloro benzylalcohol, and 4-nitro benzylalcohol, whereas electron-donating groups like methyl-, *tert*-butyl-, and methoxy-groups afforded higher TOFs. Note that the catalyst activity for most aliphatic alcohols was one order of magnitude lower compared with aromatic alcohols. Secondary aliphatic alcohols showed a higher TOF compared with primary aliphatic alcohols, with surprisingly high TOFs for 3-octanol, cyclohexanol, and 4-methyl cyclohexanol [18]. However, with longer reaction time (higher conversion), formation of some unidentified byproducts was observed when the cyclohexanol derivatives were used as a substrate. Interestingly, the formation of byproducts like the corresponding esters was detected only when the reaction was continued after the conversion reached 100%; for example, in the case of benzyl alcohol, traces of benzylbenzoate were found under these conditions. The high activity achieved with the sterically demanding substrate 9-fluorenone resembles the values determined for other aromatic systems—except for the even higher activity observed in 1-phenylethanol oxidation. This indicates good accessibility of the active sites of the catalyst even for bulky substrates.

Table 2 compares the catalytic performance of the most active ternary mixed-oxide-supported gold catalyst with that reported for other catalysts in the aerobic oxidation of 1-phenylethanol and cinnamyl alcohol. Although the experimental conditions used in the various studies deviate somehow, a rough comparison is possible. Note that comparisons of TOF and selectivity for different catalysts must be made at similar conversion. Recently, very high TOF values were reported [24,45], albeit at relatively high temperatures. Au/CeO_2 [45] and PdAu/TiO_2 [24] afforded high TOFs in the solventless oxidation of 1-phenylethanol at $160\text{ }^\circ\text{C}$ (Table 2). For Pd-free Au/TiO_2 a $\text{TOF}_{t=0.5\text{ h}}$ of 213 h^{-1} (373 K) in the oxidation of benzyl alcohol was reported, which is considerably lower than that observed in the present work ($\text{TOF}_{t=1\text{ h}} = 316\text{ h}^{-1}$; 363 K) [24]. Table 2 shows that all Au-containing catalysts had superior activity to that of Pt-group metals. A similar tendency was observed for the oxidation of cinnamyl alcohol.

Fig. 7 shows a Hammett plot derived from the catalytic data obtained for *para*-substituted alcohols with $-\text{NO}_2$, $-\text{Cl}$, $-\text{CH}_3$, and $-\text{OCH}_3$ groups. The experimental data are plotted versus the substituent coefficients σ and σ^+ . A worse fit ($R^2 = 0.90$, dashed line) was obtained when σ^+ was used instead of σ ($R^2 = 0.97$, solid line), indicating that no electron defect intermediate (e.g., carbocation) took part in the mechanism and

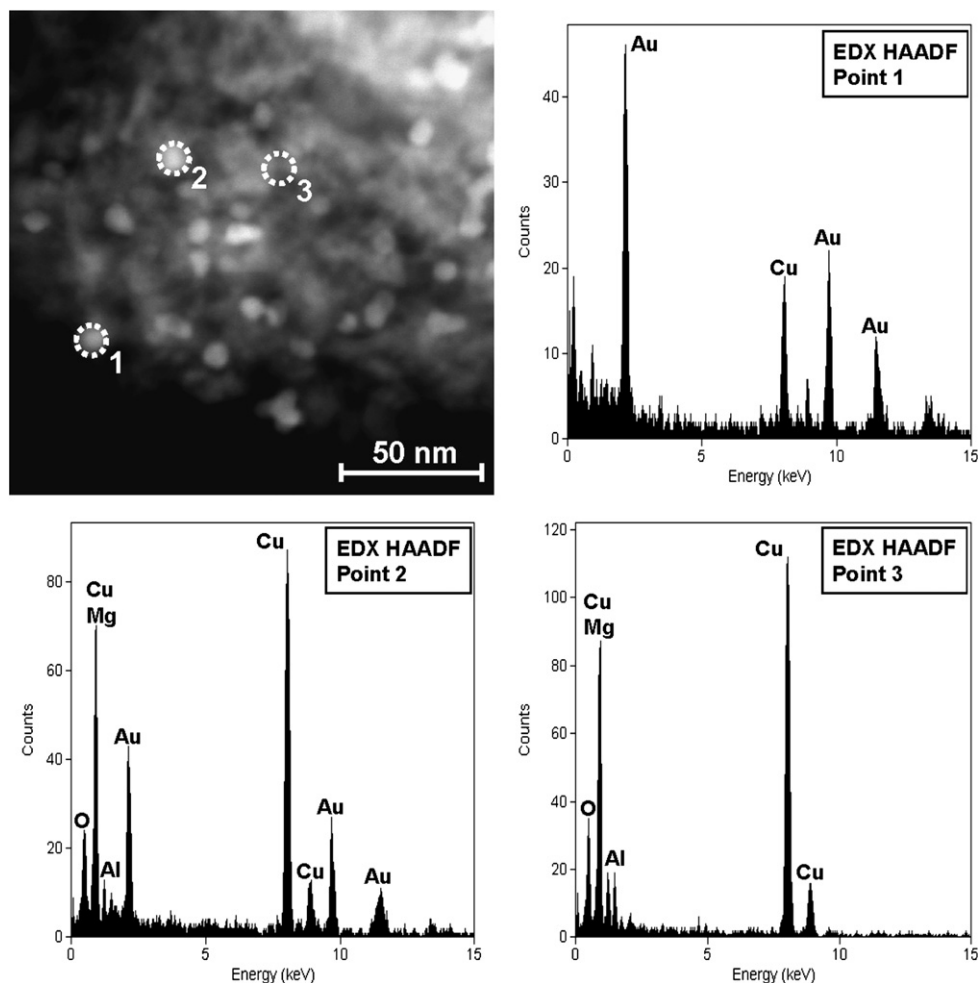


Fig. 3. Elemental mapping of the Au/Cu₅Mg₁Al₂O_x catalyst. HAADF-STEM image and EDX spectra obtained at the indicated spots. Analyses performed of particles exhibiting high brightness prove that they are gold particles. Please note that some areas of the support also appear very bright because of large thickness. In the EDX spectra, some contribution of the Cu signal is caused by the supporting Cu grid.

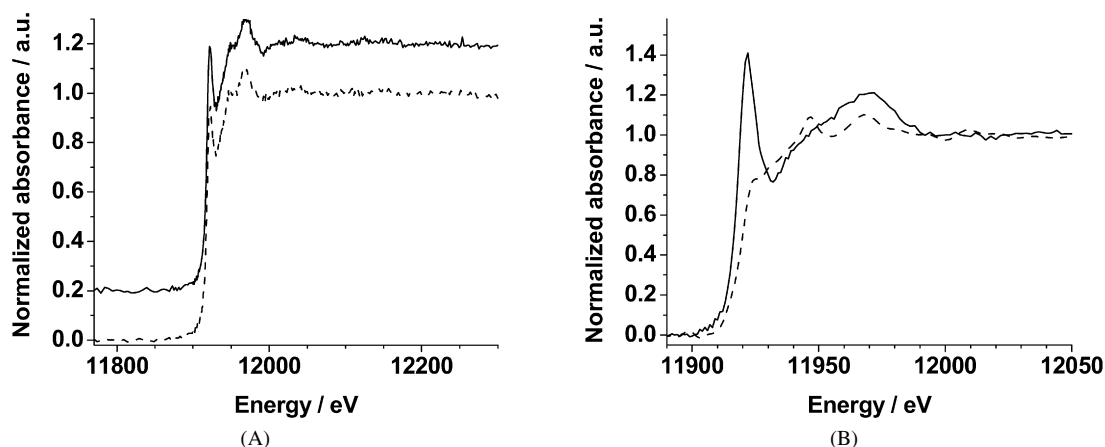


Fig. 4. XANES spectra of (A) Au/Cu₃Mg₃Al₂O_x and (B) Au/CeO₂. Spectra of fresh (solid lines) and spent catalysts (dashed lines) are shown.

that the mechanism is not a function of the substituents [56]. The increase of the reaction rate for electron-donating groups indicates that a dehydrogenation (β -hydride elimination) is the rate-limiting step. The negative value obtained ($\rho = -0.72$) is in good agreement with results obtained in the aerobic oxidation of alcohols using different alcohols [57,58].

3.3. CO₂ adsorption

As mentioned in Section 1, a base is frequently added to the reaction mixture in the catalytic aerobic oxidation of alcohols to facilitate the dehydrogenation step. ATR-IR spectroscopy was used to relate the (basic) surface properties of the catalytic ma-

Table 2

Comparison of the catalytic performance of the ternary mixed-oxide-supported gold catalyst $\text{Au}/\text{Cu}_5\text{Mg}_1\text{Al}_2\text{O}_x$ with that of other catalysts employed in the aerobic oxidation of alcohols (1-phenylethanol to acetophenone, cinnamyl alcohol to cinnamyl aldehyde)

Catalyst	1-Phenylethanol, TOF (h^{-1})	Selectivity (%)	Temperature (K)	Solvent	Reference
$\text{Au}/\text{Cu}_5\text{Mg}_1\text{Al}_2\text{O}_x$	11,748	>99	433	None	This work
PdAu/TiO_2	269,000	–	433	None	[24]
Au/CeO_2	12,500	>99	433	None	[23]
$\text{Ru}/\text{Al}_2\text{O}_3$	40	>99	313	PhCF_3	[64]
$\text{Ru}/\text{Al}_2\text{O}_3$	430	>99	423	None	[64]
$\text{Pd}/\text{hydroxyapatite}$	9800	–	433	None	[65]
$\text{Pd}/\text{hydroxyapatite}$	495	98	363	PhCF_3	[65]
$\text{Pt-Bi}/\text{Al}_2\text{O}_3$	340	>99	333	$\text{H}_2\text{O} + \text{detergent}$	[66]

Catalyst	Cinnamyl alcohol, TOF (h^{-1})	Selectivity (%)	Temperature (K)	Solvent	Reference
$\text{Au}/\text{Cu}_5\text{Mg}_1\text{Al}_2\text{O}_x$	243	99	363	Mesitylene	This work
PdAu/TiO_2	97	100	363	None	[24]
$\text{Ru}/\text{Al}_2\text{O}_3$	27	98	356	PhCF_3	[64]
$\text{Pt-Bi}/\text{Al}_2\text{O}_3$	144	>99	313	$\text{H}_2\text{O} + \text{detergent}$	[32]

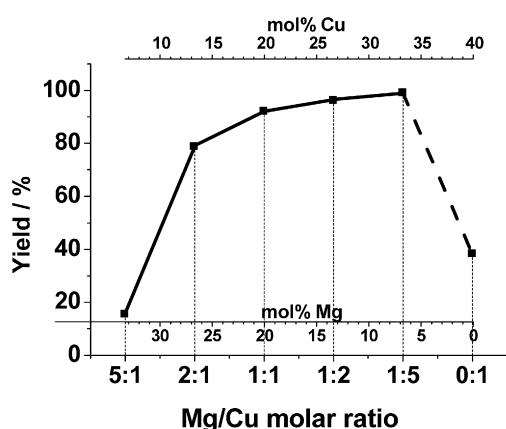


Fig. 5. Yield of phenyl-methyl ketone in aerobic oxidation of 1-phenylethanol over gold deposited on mixed-oxide supports containing different amounts of Cu, Mg, and Al. Supports vary in Mg/Cu molar ratio, while the molar ratio $(\text{Mg} + \text{Cu})/\text{Al} = 3$ is constant. Conditions: 90°C , 50 mg catalyst, 2 mmol 1-phenylethanol; formation of byproducts was not observed.

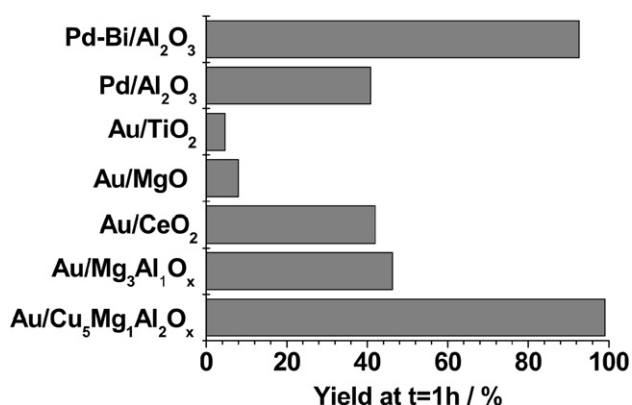


Fig. 6. Comparison of the catalytic behavior of $\text{Au}/\text{Cu}_5\text{Mg}_1\text{Al}_2\text{O}_x$ with various reference catalysts in the oxidation of 1-phenylethanol. Yield of phenyl-methyl ketone after 1 h. Note that the noble metal loading was 0.6 ± 0.17 wt% except for 1.5 wt% Au/TiO_2 and 5 wt% $\text{Pd}/\text{Al}_2\text{O}_3$. The Bi loading in $\text{Pd-Bi}/\text{Al}_2\text{O}_3$ was 0.75 wt%. Conditions: 90°C , 50 mg catalyst, 2 mmol, 1-phenylethanol; formation of byproducts was not observed.

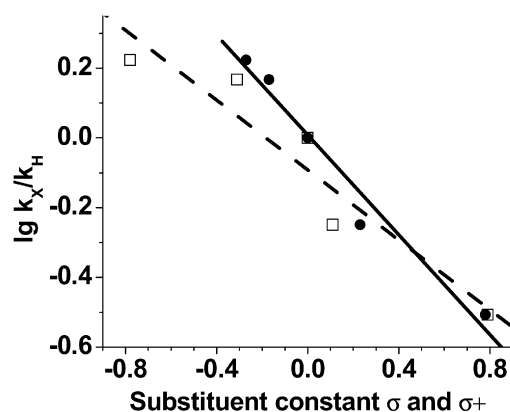


Fig. 7. Hammett plot obtained from the catalytic data of *para*-substituted benzyl alcohols. The σ (full circles) and σ^+ values (open squares) were taken from [56]. The data obtained for the fit was $\rho = -0.72$ ($R^2 = 0.97$) for the least-square fit versus σ (solid line) and $\rho = -0.50$ ($R^2 = 0.90$) for the least-square fit versus σ^+ (dashed line).

materials presented here to the catalytic performance. CO_2 adsorption from the liquid phase was studied with the aim of gaining information about the basic sites and their dependence on the support composition. The adsorption of CO_2 resulted in the formation of carbonates.

Decreasing the symmetry causes a split in the asymmetric CO stretching [59]. The magnitude of the splitting depends strongly on the binding of the carbonate (e.g., monodentate or bidentate). Whereas symmetric carbonates do not exhibit splitting in the asymmetric CO stretching, monodentate species show $\Delta\nu = 100 \text{ cm}^{-1}$ and bidentate carbonates show $\Delta\nu = 300 \text{ cm}^{-1}$. Along with the type of carbonate present, the polarization and metal bonding [59,60] strongly affect the magnitude of the splitting, with the polarization representing the dominant contribution [61].

The vibrational signals detected when investigating the materials with different Cu/Mg molar ratios were analyzed. Interpretation of the spectra is based on pertinent reports [59,62,63].

Table 3
Vibrational bands observed upon adsorption of CO₂ on various materials, data taken from references [59,62,63]

	[59]	[62]	[63]
Bidentate	1670–1625 cm ^{-1a}	1710–1660 cm ^{-1d}	1670–1600 cm ^{-1e}
	1330–1275 cm ^{-1a}	1355–1335 cm ^{-1d}	1310–1280 cm ^{-1e}
	1005–950 cm ^{-1a}		1050–980 cm ^{-1e}
Monodentate	1730–1652 cm ^{-1b}		
	1354–1234 cm ^{-1b}		
	1500 cm ^{-1c}		
Carboxylates	1565–1360 cm ^{-1c}		1630–1570 cm ^{-1e}
			1390–1350 cm ^{-1e}
			1225 cm ^{-1e}
Bicarbonate		1665–1660 cm ^{-1d}	3600 cm ^{-1e}
		1448–1430 cm ^{-1d}	1630–1615 cm ^{-1e}
		1240–1225 cm ^{-1d}	1500–1400 cm ^{-1e}

^a MgO.

^b Al₂O₃.

^c CuO.

^d MgAl₂O₄.

^e General assignment.

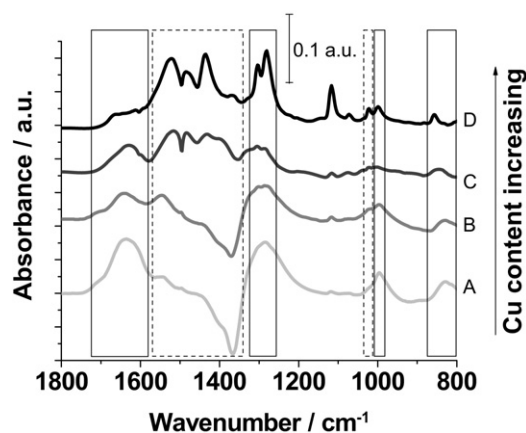


Fig. 8. ATR-IR spectra recorded after flowing CO₂-saturated toluene for 1 h over different catalysts. The Cu content is increasing from bottom (A, light gray line) to top (D, black line) with the sample presented on the bottom containing no Cu and the sample on the top (D, black line) containing no Mg, but always keeping the (Cu + Mg)/Al = 3 molar ratio constant. (A, light gray) Au/Mg₃Al₁O_x; (B, gray) Au/Cu₁Mg₅Al₂O_x; (C, dark gray) Au/Cu₅Mg₁Al₂O_x; (D, black) Au/Cu₃Al₁O_x. The regions assigned to bidentate species are marked with a solid rectangle, the regions showing monodentate species are framed with a dashed rectangle. Conditions: 80 °C, flow rate 0.56 mL/min.

The bands assigned in the aforementioned references are summarized in Table 3.

On the samples reported in the present work, only monodentate and bidentate species could be unambiguously identified. The presence of bicarbonates, bridged species, and formates was excluded due to missing signals in the corresponding re-

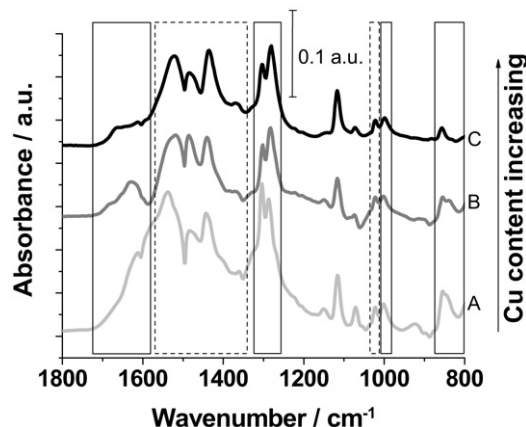


Fig. 9. Spectra recorded after flowing CO₂-saturated toluene for 1 h over different supported gold catalysts. The Cu content is increasing from bottom (A, light gray line) to top (C, black line) with the sample presented on the bottom containing no Cu: (A, light gray line) Au/CeO₂; (B, gray line) Au/20 wt% CuO/CeO₂; and (C, black line) Au/Cu₃Al₁O_x. Conditions: 80 °C, flow rate 0.56 mL/min.

gions [63]. However, due to the high similarity between carboxylates and monodentate carbonates, the possibility that carboxylates were also present cannot be excluded. Monodentate carbonates are bound to the surface via the positively polarized CO₂–carbon atom and a Lewis base on the surface, possibly an anionic oxygen species. Carboxylates, on the other hand, are a form of bidentate carbonates in which the CO₂ is bound to the surface at a Lewis acid site via its negatively polarized oxygen atoms. Bidentate species exhibit both features; one binding is established between the CO₂–carbon atom and a surface oxygen atom, and the other binding occurs between a CO₂–oxygen and a Lewis acid site involving possibly Mg, Al, or Cu. A clear assignment regarding bidentate and monodentate species can be made. The vibrational bands observed are summarized in Table 4 and the corresponding spectra, recorded after 1 h of adsorption from CO₂-saturated toluene, are shown in Fig. 8.

The addition of Cu produced more complex spectra. The copper component changed the pattern of the sites able to adsorb CO₂ from mostly strong adsorption sites binding CO₂ in a bidentate manner to adsorption sites showing monodentate-binding properties. In the region typical for the appearance of monodentate carbonates, numerous very well separated, sharp signals were identified. However, a possible overlap of the signals of interest with signals being assigned to toluene can lead to an apparent splitting. Thus, the sharp negative bands at 1494 and 1455 cm⁻¹ might be caused by incomplete compensation of the solvent signals in presence of toluene saturated with CO₂. (The background was recorded while flowing N₂-saturated toluene.) The bands identified at 1487 and 1389 cm⁻¹ are possibly only shoulders of a larger carbonate envelope overlapping with the spectrum of toluene.

Similar findings emerged from the analysis of Au on pure CeO₂ and Au nanoparticles on 20 wt% CuO/CeO₂ (Fig. 9). Whereas the pure CeO₂ exhibited a strong signal above $\nu > 1600$ cm⁻¹ (Fig. 9A, light-gray line) assigned to bidentate species, this signal decreased with increasing Cu content, as can be seen for the support 20 wt% CuO/CeO₂ (Fig. 9B, gray

Table 4
Vibrational signals (cm^{-1}) observed upon adsorption of CO_2 from CO_2 -saturated toluene by means of ATR-IR spectroscopy

	Bidentate carbonates (cm^{-1})		Monodentate carbonates (cm^{-1})				
Au/ $\text{Mg}_3\text{Al}_1\text{O}_x$	1649	1287	998	826			
Au/ $\text{Cu}_1\text{Mg}_5\text{Al}_2\text{O}_x$	1641	1302sh/1287	995	831	1546	1443sh	1023
Au/ $\text{Cu}_5\text{Mg}_1\text{Al}_2\text{O}_x$	1632w	1304/1293	998	846	1516/1485	1431/1394sh	1023
Au/ $\text{Cu}_3\text{Al}_1\text{O}_x$	1656w/1610w	1304/1294	998	856	1520/1484	1435/1372	1021
Au/ CeO_2	1680sh/1614	1304/1286	998	854	1548	1442	1020
Au/20 wt% CuO/ CeO_2	1680sh/1631	1304/1286	998	855	1517/1482	1441	1022

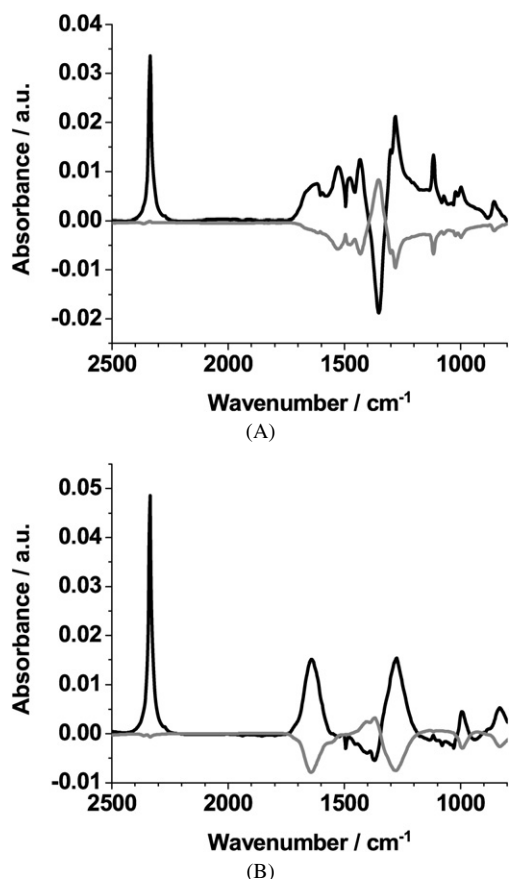


Fig. 10. In phase (0° , black line) and out of phase (90° , gray line) spectra recorded for the samples Au/ $\text{Cu}_5\text{Mg}_1\text{Al}_2\text{O}_x$ (A) and $\text{Mg}_3\text{Al}_1\text{O}_x$ (B). The stimulation periods were 408.2 s (A) and 1431.5 s (B) resulting in a frequency of 2.4 mHz and 0.7 mHz, respectively. Conditions: 80°C , flow rate 0.56 mL/min.

line). The spectrum recorded for Au/ $\text{Mg}_3\text{Al}_1\text{O}_x$ (Fig. 8D, black line) is plotted for comparison. The shift from a surface largely populated by bidentate species toward a surface covered predominantly by CO_2 bound as monodentate species is evident for the copper-containing catalyst.

To further elucidate the origin and features of the negative signal (1370 cm^{-1}), modulation experiments were performed. The results show that this signal was negatively correlated with respect to the carbonate signals for all materials investigated (Fig. 10). The contribution of this negative signal depended on the Mg content of the mixed-oxide supports; its intensity decreased in the sample with lower Mg content, and it was not observed for the Mg-free sample (Fig. 10A). It was also absent in the Au/ MgO . However, the contribution of the signal at $\nu = 1370\text{ cm}^{-1}$ —especially for the Cu-free sample depicted

in Fig. 10B—was strongly diminished by employing the MES approach. The intensities affected by the modulation corresponded to the signals identified during the adsorption of CO_2 . Note that the signal at 1370 cm^{-1} was negatively correlated with respect to the monodentate and bidentate species identified during CO_2 adsorption. This signal is possibly due to carbonaceous species present on the surface or to basic magnesium carbonate present on the support. However, due to the information gained from MES, it can be concluded that the appearance of this signal is caused by another surface species other than the monodentate and bidentate carbonates. Whereas the CO_2 adsorption studies clearly revealed significant changes in the basic surface properties on Cu promotion, whether these changes are at the origin of the enhanced activity of the ternary mixed-oxide-supported gold catalyst remains unclear. The enhanced activity may be the result of several superimposed contributions, such as surface basicity, redox properties of Cu, and the oxidation state of Au, as well as the possible effect of Cu on gold particle size. Further investigations aiming at discriminating among these contributions, particularly under in situ conditions, are needed to gain a thorough understanding of the promotional effect observed.

4. Conclusion

In this study, binary and ternary mixed oxides containing Mg–Al, Cu–Al, and Cu–Mg–Al were prepared by FSP and applied as supports for Au nanoparticles. The mixed oxides showed similar textural properties, characterized by low porosity in the micropore and lower-mesopore regions and similar BET surface areas. Gold particles with diameter ranging from 6 to 9 nm were deposited on the supports by deposition–precipitation. The gold loading amounted to $0.6 \pm 0.17\text{ wt}\%$. The various supported gold catalysts were tested in the aerobic oxidation of 1-phenylethanol; the best catalytic performance was achieved for a ternary mixed-oxide-supported gold catalyst with the composition Au/ $\text{Cu}_5\text{Mg}_1\text{Al}_2\text{O}_x$. The Cu- and Mg-containing mixed oxide led to strongly enhanced activity of the supported gold nanoparticles, demonstrating these constituents' important roles as promoters. This catalyst was tested in the oxidation of various structurally different alcohols. For most of the alcohols, full conversion was achieved at high selectivity ($\geq 98\%$). The ternary mixed-oxide-supported gold catalyst, Au/ $\text{Cu}_5\text{Mg}_1\text{Al}_2\text{O}_x$, showed significantly higher activity for the oxidation of several alcohols under similar conditions compared with various pertinent reference catalysts (i.e., Au/ CeO_2 , Pd/ Al_2O_3 , Bi-promoted Pd/ Al_2O_3).

CO₂ adsorption from the liquid phase combined with ATR-IR spectroscopy revealed different monodentate and bidentate carbonate species as major surface species. The population of monodentate species increased with increasing Cu content of the supports, indicating a change of surface basicity on Cu promotion. This tendency was observed for both ternary mixed oxides and binary CuO/CeO₂ supports. Ex situ XANES of the fresh and spent catalyst revealed that a significant fraction of the deposited gold existed as charged species. Final assessment of the role of these species in the catalytic process will require in situ measurements, which are the subject of a forthcoming study.

Acknowledgments

The authors thank Frank Krumeich for the electron microscopy investigations performed at the electron microscopy center of ETH Zurich (EMEZ), Dr. Tamas Mallat for his fruitful comments on the manuscript, and Dr. Davide Ferri for his support during ATR-IR measurements. P.H. gratefully appreciates the fruitful discussions with Dr. Atsushi Urakawa and Dr. Ronny Wirz during the MES experiments and assistance from Niels van Vegten in the FSP application. Zsuzsanna Opre is acknowledged for sharing her experience in aerobic alcohol oxidation and GC analysis. The authors also thank ANKA for providing beamtime for the studies. Financial support by the EU under contract RII3-CT-2004-506008 (IA-SFS) is gratefully acknowledged.

References

- [1] A.S.K. Hashmi, G.J. Hutchings, *Angew. Chem. Int. Ed.* 45 (2006) 7896.
- [2] M. Haruta, *CATTECH* 6 (2002) 102.
- [3] M. Haruta, N. Yamada, T. Kobayashi, S. Iijima, *J. Catal.* 115 (1989) 301.
- [4] J.D. Grunwaldt, C. Kiener, C. Wogerbauer, A. Baiker, *J. Catal.* 181 (1999) 223.
- [5] J.D. Grunwaldt, M. Maciejewski, O.S. Becker, P. Fabrizioli, A. Baiker, *J. Catal.* 186 (1999) 458.
- [6] J.K. Edwards, B.E. Solsona, P. Landon, A.F. Carley, A. Herzing, C.J. Kiely, G.J. Hutchings, *J. Catal.* 236 (2005) 69.
- [7] M.D. Hughes, Y.J. Xu, P. Jenkins, P. McMorn, P. Landon, D.I. Enache, A.F. Carley, G.A. Attard, G.J. Hutchings, F. King, E.H. Stitt, P. Johnston, K. Griffin, C.J. Kiely, *Nature* 437 (2005) 1132.
- [8] A.K. Sinha, S. Seelan, T. Akita, S. Tsubota, M. Haruta, *Appl. Catal. A Gen.* 240 (2003) 243.
- [9] B. Taylor, J. Lauterbach, W.N. Delgass, *Appl. Catal. A Gen.* 291 (2005) 188.
- [10] C. Bianchi, F. Porta, L. Prati, M. Rossi, *Top. Catal.* 13 (2000) 231.
- [11] L. Prati, F. Porta, *Appl. Catal. A Gen.* 291 (2005) 199.
- [12] L. Prati, M. Rossi, *J. Catal.* 176 (1998) 552.
- [13] S. Carrettin, P. McMorn, P. Johnston, K. Griffin, G.J. Hutchings, *Chem. Commun.* (2002) 696.
- [14] S. Biella, G.L. Castiglioni, C. Fumagalli, L. Prati, M. Rossi, *Catal. Today* 72 (2002) 43.
- [15] M. Comotti, C. Della Pina, R. Matarrese, M. Rossi, *Angew. Chem. Int. Ed.* 43 (2004) 5812.
- [16] C. Baatz, U. Prüsse, *Catal. Today* (2007), doi:10.1016/j.cattod.2006.12.004, in press.
- [17] N. Thielecke, M. Aytemir, U. Prüsse, *Catal. Today* 121 (2007) 115.
- [18] T. Mallat, A. Baiker, *Chem. Rev.* 104 (2004) 3037.
- [19] C. Keresszegi, T. Mallat, J.D. Grunwaldt, A. Baiker, *J. Catal.* 225 (2004) 138.
- [20] F. Cavani, F. Trifiro, A. Vaccari, *Catal. Today* 11 (1991) 173.
- [21] J.I. Di Cosimo, V.K. Diez, M. Xu, E. Iglesia, C.R. Apesteguia, *J. Catal.* 178 (1998) 499.
- [22] A. Corma, V. Fornes, F. Rey, *J. Catal.* 148 (1994) 205.
- [23] A. Abad, P. Concepcion, A. Corma, H. Garcia, *Angew. Chem. Int. Ed.* 44 (2005) 4066.
- [24] D.I. Enache, J.K. Edwards, P. Landon, B. Solsona-Espriu, A.F. Carley, A.A. Herzing, M. Watanabe, C.J. Kiely, D.W. Knight, G.J. Hutchings, *Science* 311 (2006) 362.
- [25] D.I. Enache, D.W. Knight, G.J. Hutchings, *Catal. Lett.* 103 (2005) 43.
- [26] M. Comotti, C. Della Pina, M. Rossi, *J. Mol. Catal. A Chem.* 251 (2006) 89.
- [27] C.H. Christensen, B. Jorgensen, J. Rass-Hansen, K. Egeblad, R. Madsen, S.K. Klitgaard, S.M. Hansen, M.R. Hansen, H.C. Andersen, A. Riisager, *Angew. Chem. Int. Ed.* 45 (2006) 4648.
- [28] M. Crivello, C. Perez, E. Herrero, G. Ghione, S. Casuscelli, E. Rodriguez-Castellon, *Catal. Today* 107–108 (2005) 215.
- [29] L. Mädler, H.K. Kammler, R. Müller, S.E. Pratsinis, *J. Aerosol Sci.* 33 (2002) 369.
- [30] L. Mädler, W.J. Stark, S.E. Pratsinis, *J. Mater. Res.* 17 (2002) 1356.
- [31] T. Mallat, Z. Bodnar, A. Baiker, O. Greis, H. Strubig, A. Keller, *J. Catal.* 142 (1993) 237.
- [32] T. Mallat, Z. Bodnar, P. Hug, A. Baiker, *J. Catal.* 153 (1995) 131.
- [33] D. Günther, R. Frischknecht, C.A. Heinrich, H.J. Kahlert, *J. Anal. At. Spectrom.* 12 (1997) 939.
- [34] D. Günther, C.A. Heinrich, *J. Anal. At. Spectrom.* 14 (1999) 1363.
- [35] Z. Opre, J.D. Grunwaldt, M. Maciejewski, D. Ferri, T. Mallat, A. Baiker, *J. Catal.* 230 (2005) 406.
- [36] D. Baurecht, I. Porth, U.P. Fringeli, *Vib. Spectrosc.* 30 (2002) 85.
- [37] D. Baurecht, U.P. Fringeli, *Rev. Sci. Instrum.* 72 (2001) 3782.
- [38] T. Bürgi, A. Baiker, *Adv. Catal.* 50 (2006) 227.
- [39] T. Bürgi, A. Baiker, *J. Phys. Chem. B* 106 (2002) 10649.
- [40] A. Urakawa, R. Wirz, T. Bürgi, A. Baiker, *J. Phys. Chem. B* 107 (2003) 13061.
- [41] J.D. Grunwaldt, S. Hannemann, J. Göttlicher, S. Mangold, M.A. Denecke, A. Baiker, *Phys. Scr.* 2005 (2005) 769.
- [42] R. Jossen, S.E. Pratsinis, W.J. Stark, L. Mädler, *J. Am. Ceram. Soc.* 88 (2005) 1388.
- [43] W.J. Stark, L. Mädler, M. Maciejewski, S.E. Pratsinis, A. Baiker, *Chem. Commun.* (2003) 588.
- [44] A. Abad, C. Almela, A. Corma, H. Garcia, *Chem. Commun.* (2006) 3178.
- [45] A. Abad, C. Almela, A. Corma, H. Garcia, *Tetrahedron* 62 (2006) 6666.
- [46] S. Carrettin, P. McMorn, P. Johnston, K. Griffin, C.J. Kiely, G.J. Hutchings, *Phys. Chem. Chem. Phys.* 5 (2003) 1329.
- [47] P. Zhang, T.K. Sham, *Phys. Rev. Lett.* 90 (2003).
- [48] R.E. Benfield, D. Grandjean, M. Kroll, R. Pugin, T. Sawitowski, G. Schmid, *J. Phys. Chem. B* 105 (2001) 1961.
- [49] P. Zhang, T.K. Sham, *Appl. Phys. Lett.* 81 (2002) 736.
- [50] I.W. Bassi, F.W. Lytle, G. Parravano, *J. Catal.* 42 (1976) 139.
- [51] J.W. Watkins, R.C. Elder, B. Greene, D.W. Darnall, *Inorg. Chem.* 26 (1987) 1147.
- [52] I. Berrodier, F. Farges, M. Benedetti, M. Winterer, J.G.E. Brown, M. Devueghele, *Geochim. Cosmochim. Acta* 68 (2004) 3019.
- [53] A. Pantelouris, G. Kuper, J. Hormes, C. Feldmann, M. Jansen, *J. Am. Chem. Soc.* 117 (1995) 11749.
- [54] C. Keresszegi, J.D. Grunwaldt, T. Mallat, A. Baiker, *Chem. Commun.* (2003) 2304.
- [55] C. Keresszegi, J.D. Grunwaldt, T. Mallat, A. Baiker, *J. Catal.* 222 (2004) 268.
- [56] T.H. Lowry, K.S. Richardson, *Mechanism Theory on Organic Chemistry*, third ed., Harper & Row, New York, 1987.
- [57] J.A. Mueller, C.P. Goller, M.S. Sigman, *J. Am. Chem. Soc.* 126 (2004) 9724.
- [58] Z. Opre, D. Ferri, F. Krumeich, T. Mallat, A. Baiker, *J. Catal.* 241 (2006) 287.
- [59] G. Busca, V. Lorenzelli, *Mater. Chem.* 7 (1982) 89.
- [60] R.E. Hester, W.E. Grossman, *Inorg. Chem.* 5 (1966) 1308.
- [61] B. Taravel, P. Delorme, G. Chauvet, V. Lorenzelli, *J. Mol. Struct.* 13 (1972) 283.

- [62] C. Morterra, G. Ghiotti, F. Boccuzzi, S. Coluccia, *J. Catal.* 51 (1978) 299.
- [63] A.M. Turek, I.E. Wachs, E. Decanio, *J. Phys. Chem.* 96 (1992) 5000.
- [64] K. Yamaguchi, N. Mizuno, *Angew. Chem. Int. Ed.* 41 (2002) 4538.
- [65] K. Mori, K. Yamaguchi, T. Hara, T. Mizugaki, K. Ebitani, K. Kaneda, *J. Am. Chem. Soc.* 124 (2002) 11572.
- [66] T. Mallat, Z. Bodnar, A. Baiker, *Stud. Surf. Sci. Catal.* 78 (1993) 377.